Journal of Power Sources 196 (2011) 140–146

Contents lists available at ScienceDirect

Journal of Power Sources

journal homepage: www.elsevier.com/locate/jpowsour

Corrosion of carbon support for PEM fuel cells by electrochemical quartz crystal microbalance

Chih-Cheng Hung[a], Pau-Yee Lim[b], Jiann-Ruey Chen[a], Han C. Shih[a,c,*]

[a] Department of Materials Science and Engineering, National Tsing Hua University, Hsinchu 300, Taiwan
[b] Material and Chemical Research Laboratories, Industrial Technology Research Institute, Bldg. 77,195, Sec. 4, Chung Hsing Rd., Chutung, Hsinchu 310, Taiwan
[c] Institute of Materials Science and Nanotechnology, Chinese Culture University, Taipei 111, Taiwan

ARTICLE INFO

Article history:
Received 28 April 2010
Received in revised form 6 July 2010
Accepted 7 July 2010
Available online 13 July 2010

Keywords:
Corrosion
Electrochemical quartz crystal microbalance
Carbon support
Carbon black
PEMFC
Fuel cells

ABSTRACT

During the voltammetry of carbon supports for proton exchange membrane fuel cells (PEMFCs), including commercial carbon blacks, graphitized carbon black and multi-wall carbon nanotubes (MWNTs), in deaerated 0.5 M H_2SO_4 solution results in mass changes as observed by using in situ electrochemical quartz crystal microbalance (EQCM). The mass change and corrosion onset potential during electrochemical carbon corrosion indicate that oxides are formed and accumulated on the carbon surface, leading to an increase in mass. A decrease in the mass is associated with carbon loss from the gasification of carbon surface oxides into carbon dioxide. High BET surface area carbon blacks ECP600 and ECP 300 have a carbon loss of 0.0245 ng cm^{-2} s^{-1} and 0.0144 ng cm^{-2} s^{-1} and as compared to 0.0115 ng cm^{-2} s^{-1} for low surface area support XC-72 and so they are less resistant to corrosion. Graphitized XC-72 and MWNTs, with higher graphitization have higher carbon corrosion onset potential at 1.65 V and 1.62 V and appear to be more intrinsically resistant to corrosion.

1. Introduction

Carbon-supported platinum is the most commonly used catalyst in PEMFCs. Carbon black is widely used as a support material for nano-sized platinum particles due to its low cost and other favorable properties. It possesses good chemical stability, and when used as support material, it provides several desired functions, such as electronic continuity, a high surface area that enables a uniform dispersion of Pt nanoparticles, and a porous structure that facilitates the mass transportation of reactant and reaction products [1]. However, recent studies have reported that adverse effects arise from oxidation and corrosion of the carbon support in PEMFCs at the higher potential region near the open circuit voltage. It was observed that the surface groups that form during carbon oxidation change the surface properties of the carbon support. This may cause an increase in surface hydrophilicity, leading to the flooding effect, which could impede mass transport within the catalyst layer [2]. Furthermore, such surface oxidation can be accelerated due to the presence of the Pt catalyst. As a result, the Pt particles attached to the carbon surface eventually become detached due to loss of carbon [3]. Loss of carbon could decrease the electronic continuity of the catalyst layer, aggravate aggregation of isolated Pt particles and reduces the electrochemically active surface area of Pt [4–6]. Consequently, carbon support corrosion is considered to be one of the most serious problems facing the performance and lifetime of PEMFCs.

From a thermodynamic perspective, carbon can be corroded to carbon dioxide at a potential above 0.207 V (vs. NHE) [7]. The electrochemical reaction is shown in Eq. (1).

$$C + 2H_2O = CO_2 + 4H^+ + 4e^-, E^0 = 0.207\,V_{NHE} \quad (1)$$

In a PEMFC, the carbon support at the anode is comparatively more stable than cathode. The cathode side carbon support tends to corrode due to high oxygen concentration, low pH and a high operation potential between 0.6 V and 1 V. Some situations, such as during shutdown and restart, can cause the local potential at the cathode to be even higher than 1.5 V. These abnormal situations enhance carbon corrosion [8,9].

Carbon corrosion is generally analyzed by simple cyclic voltammetry (CV) measurements. The accumulation of surface oxide can then be estimated from the CV curves [10]. However, the results from CV are equivocal because the actual mass loss of carbon during corrosion is disregarded [11]. In some cases, studies on carbon corrosion for PEMFCs involve the use of mass spectrometry [12–14] or non-dispersive infrared spectroscopy [15] to monitor the gener-

* Corresponding author at: Department of Materials Science and Engineering, National Tsing Hua University, Hsinchu 300, Taiwan. Tel.: +886 3 5715131x3845; fax: +886 3 5710290.
E-mail address: hcshih@mx.nthu.edu.tw (H.C. Shih).

0378-7753/$ – see front matter © 2010 Published by Elsevier B.V.
doi:10.1016/j.jpowsour.2010.07.015

ation of CO_2 under electrochemical oxidation conditions. However, complicated experimental tools are needed that allow the direct measurement of the CO_2 evolution rate from the membrane-electrode-assembly (MEA) sample, which is composed of not only the carbon support but also carbon cloth/paper.

The electrochemical quartz crystal microbalance (EQCM) is a sensitive instrument that allows measurements of mass changes in the nanogram range in electrochemical systems [16]. Yadav et al. [17] used EQCM combined with the CV method to investigate carbon oxidation of a sputtered carbon electrode. They observed mass loss during the CV positive scan. Dam et al. [18] used EQCM to evaluate the stability of XC-72 under several potentiostatic conditions at elevated temperatures and suggested that the sharp drop in mass at potentials higher than 1.15 V (vs. NHE) could be due to the formation of CO_2.

In this work, we investigate the carbon corrosion of various types of carbon support materials for PEMFCs, including the widely used commercial carbon blacks, graphitized carbon black and multi-wall carbon nanotubes. The EQCM method combined with CV in a three-electrode system was employed to investigate in situ mass change due to carbon corrosion during a positive CV scan between 0 V and 1.2 V. This work also demonstrates the influence of the BET surface area on carbon loss and on the inhibition of carbon corrosion at higher graphitization degrees.

2. Experimental

2.1. Sample preparation

Commercial carbon blacks: Vulcan XC-72 (Cabot), Ketjen black ECP300 (Akzo Nobel Chemicals), Ketjen black ECP600 (Akzo Nobel Chemicals), graphitized XC-72 and MWNTs were used to prepare carbon film quartz crystal electrodes (C-QCEs) for EQCM measurements. The commercial carbon blacks and MWNTs were used as received. The graphitized XC-72 was prepared by high-temperature heat treatment in a high-temperature furnace. The XC-72 was heated from an ambient temperature to 2200 °C and held at that temperature for 60 min. The furnace was purged with dry argon before and during the heating process. The carbons were ultrasonically mixed in isopropanol (IPA), with a carbon to IPA weight ratio of 1:200, to form well-dispersed carbon inks. A T-cut 7.995 MHz Au-coated quartz crystal electrode (Au-QCE) with an area of 0.196 cm^2 was used as a working electrode substrate. The C-QCE was prepared by spray coating a fixed amount of well-dispersed carbon inks to obtain about 10 μg of carbon on the Au-QCE. A Teflon mask that pre-covered the Au-QCE was used for the confined coating area. After the coating process, the C-QCE was oven-dried at 65 °C for 1 h.

2.2. Electrochemical experiment

Resonance frequencies were measured using an EG&G PAR model QCA917 to evaluate the mass change. The relation between the change in resonance frequency and the mass change on the quartz crystal electrode was calculated by the Sauerbrey equation:

$$\Delta f = \frac{-2nf^2}{\sqrt{\mu_q \rho_q}} \frac{\Delta m}{A}, \quad (2)$$

where Δf is the measured resonant frequency change (Hz), n is the fundamental mode of the crystal, f is the resonant frequency of the fundamental mode of the crystal, μ_q is the shear modulus of quartz (2.947×10^{11} g cm^{-1} s^{-2}), ρ_q is the density of quartz (2.684 g cm^{-3}), Δm is the mass change, and A is the area of the gold disk coated on the crystal. This equation was used to calculate the mass change from the frequency change, neglecting the small viscous effects observed. In our measurements, a net change of 1 Hz corresponds to 1.34 ng of mass change on the crystal surface area of 0.196 cm^2. QCE frequencies were measured before and after carbon spray coating to record the weight of the deposited carbon. The amount of deposited carbon was maintained at about 10 μg, less than 2% of the unloaded quartz crystal, so that the Sauerbrey equation could be used accurately [19]. The mass change response from EQCM data in this study was calculated and normalized to the initial carbon black's sample mass.

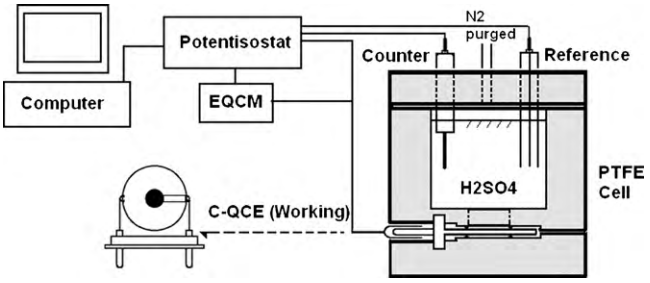

Fig. 1. Schematic of the EQCM system.

A standard, three-electrode cell, with a C-QCE as the working electrode, a hydrogen reference electrode and a platinum wire as the counter electrode, was used in an electrochemical experiment. The electrodes positioned in a Teflon-made cell were connected to the EG&G PAR model QCA917 and an EG&G PAR model 263A potentiostat for the EQCM measurements. The assembly is shown in Fig. 1. All tests were carried out at room temperature in a 0.5 M H_2SO_4 solution that was purged with nitrogen for 30 min to remove dissolved oxygen. Prior to the EQCM measurements, the C-QCE working electrode was pre-activated first by immersion in the deaerated 0.5 M H_2SO_4 solution for 24 h, and subsequently by electrochemical potential cycling between 0.05 V and 1.2 V at a scan rate of 50 mV s^{-1} until the resultant CV curves became stable.

2.3. Physical characterization

The graphitization degree of the carbon materials was characterized with a Raman spectrometer (Renishaw system 2000) using a HeNe laser (632.8 nm excitation wavelength) as the light source. The specific surface area and pore volume of the carbon support was measured using a Brunauer–Emmett–Teller (BET) apparatus (Micromeritics ASAP 2010).

3. Results and discussion

3.1. EQCM measurement of XC-72

EQCM measurements of a bare Au-QCE were performed in deaerated 0.5 M H_2SO_4 at 298 K at a scan rate of 10 mV s^{-1}. Fig. 2 presents the CV and corresponding EQCM mass change data for the bare Au-QCE. Only a small mass change was observed below 0.6 V during the positive scan from 0.05 V. The notable mass gain at a potential from 0.6 V to 0.9 V could be attributed to the adsorption of sulfuric acid anions [17]. The mass increment was minimal at potentials above 0.9 V. These results were maintained until 1.4 V, at which point continuous mass gain again occurred. From this result, it was evident that the influence of mass change from the Au electrode background was negligible within the potential range of 1.0–1.4 V. Considering the possibility of oxygen evolution at the higher potential region and that carbon black may be detached mechanically from the C-QCE electrode, the upper potential range was limited to 1.2 V in subsequent CV experiments.

The XC-72 carbon film quartz crystal electrode (C-QCE) was similarly characterized by CV and EQCM in deaerated 0.5 M H_2SO_4 at a scan rate of 10 mV s^{-1}. Fig. 3 shows the CV and mass change

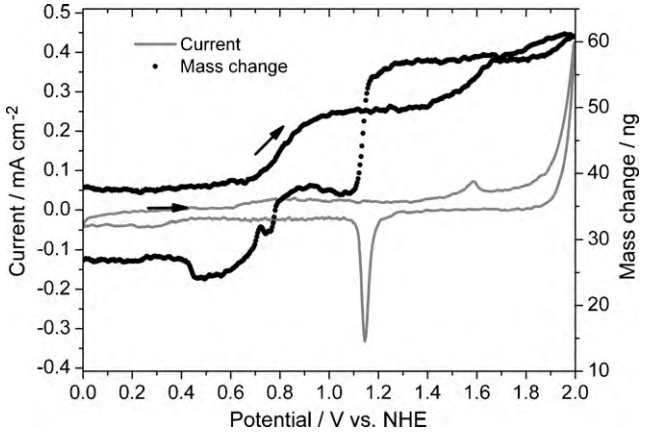

Fig. 2. The EQCM mass change responses for the bare Au quartz crystal electrode (Au-QCE) recorded simultaneously with the CV in deaerated 0.5 M H_2SO_4, at a scan rate of 10 mV s^{-1} and a temperature of 298 K.

response of the XC-72 C-QCE. The CV result for XC-72 C-QCE shows the typical CV curve of a carbon material, which evidently has a large current contribution from double layer charging. This result shows that the electrochemical experimental signal of the C-QCE was dominated by carbon and that the effect of the background Au electrode is negligible. An obvious redox peak around 0.6 V resulted from the formation of the surface oxide group hydroquinone–quinone (HQ–Q), which underwent redox reactions on the surface of carbon during carbon corrosion [20–22]. Accordingly, it was confirmed that carbon corrosion occurred under the above test conditions. From the corresponding mass change recorded, it was observed that the mass change of the XC-72 C-QCE was minimal in the range of 0–0.4 V during the positive scan. Above this potential, an obvious mass gain was observed, and this gain was accelerated above 0.65 V. The mass increased continuously until around 1.05 V, at which point the mass change reversed and sharply decreased until it reached the end of the positive scan at 1.2 V.

Electrochemical carbon corrosion in acid electrolytes occurs via a three-step process [5,23]:

Step 1: Oxidation of the carbon lattice $C_{Surf} \rightarrow C^{+}{}_{Surf} + e^{-}$
Step 2: Hydrolysis $C_{Surf} + 1/2\ H_2O \rightarrow C_{Surf}O + H^{+}$
Step 3: Gasification of surface carbon oxides to carbon dioxide: $2C_{Surf}O + H_2O \rightarrow C_{Surf}O + CO_2 + 2H^{+} + 2e^{-}$

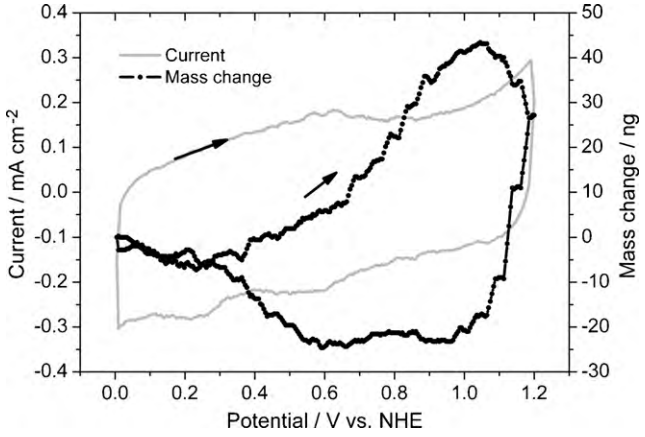

Fig. 3. The EQCM mass change responses for the Vulcan XC-72 carbon film quartz crystal electrode (C-QCE) recorded simultaneously with the CV in deaerated 0.5 M H_2SO_4 at a scan rate of 10 mV s^{-1} and a temperature of 298 K.

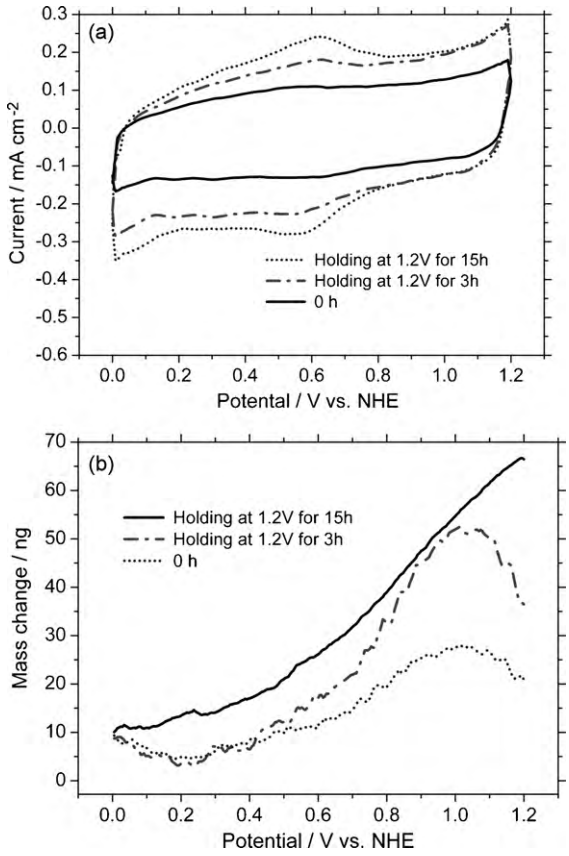

Fig. 4. (a) CV and (b) EQCM data for Vulcan XC-72 C-QCE at a scan rate of 10 mV s^{-1} in deaerated 0.5 M H_2SO_4 at 298 K after holding at a constant potential of 1.2 V for 0 h, 3 h and 15 h.

The mass change is related to the electrochemical corrosion of carbon involving the formation of surface oxides (Step 2), followed by gasification of surface carbon oxides to carbon dioxide (Step 3) [24]. The formation rate of surface oxides, $C_{Surf}O$, differed from the following oxidation to CO_2. Therefore, electrochemical carbon corrosion behavior could be observed by the mass change of the EQCM measurement. At a lower potential (below 1.05 V) in the carbon corrosion reaction, the carbon surface oxides (hydroxyl, carbonyl and carboxylic) accumulated on the carbon surface, which led to an increase in mass. Furthermore, after the HQ–Q redox reaction (~0.6 V), the carbon surface became more hydrophilic, and hence, the mass tended to increase faster with the adsorption of water. At a higher potential (above 1.05 V), the overvoltage was sufficient to accelerate the gasification of surface carbon oxides to carbon dioxide, which led to a drop in mass associated with carbon loss.

Further investigation of the carbon corrosion behavior of XC-72 C-QCE using the EQCM method was carried out during the accelerated durability test (ADT) in deaerated 0.5 M H_2SO_4. This process involved holding a constant potential of 1.2 V and cycling between 0 V and 1.2 V at scan rate of 50 mV s^{-1}. Fig. 4 shows the measured EQCM CV curves and the corresponding mass change of the XC-72 C-QCE, before and after holding the potential at 1.2 V for 3 h and 15 h. The CV curve for the freshly prepared XC-72 C-QCE shows a relatively low background current. No reaction peak is observed. After holding the potential at 1.2 V, the CV background current of surface carbon oxides increased, and the reaction peaks associated with the HQ–Q redox couple (around 0.6 V) became more distinguishable. The corresponding EQCM mass change results revealed a continuous accumulation of various species (including surface oxide) on the fresh carbon. The maximum mass gain that could be achieved during a CV scan decreased after pro-

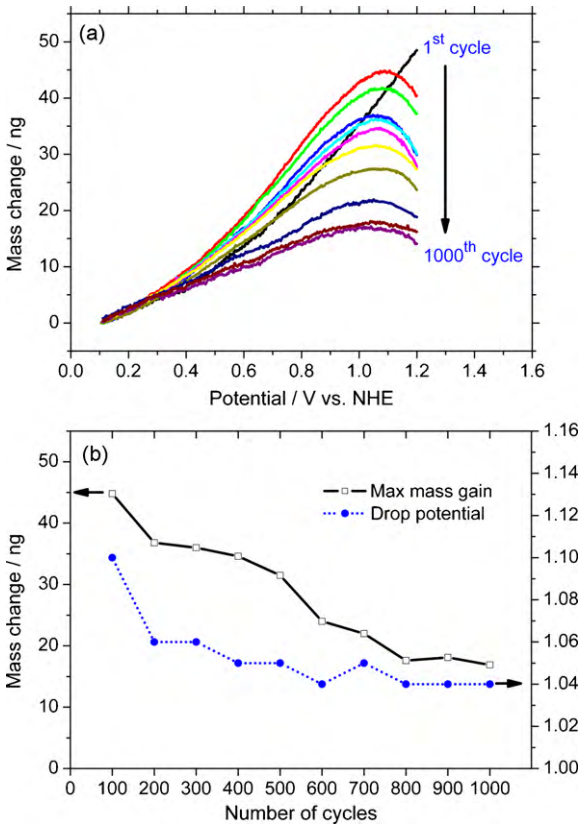

Fig. 5. (a) EQCM mass change (positive CV scan) for 1000 cycles, and (b) maximum mass gain and mass drop onset potential vs. CV cycles.

longed holding the potential at 1.2 V for 3 h and 15 h, implying higher coverage of adsorbed species on the carbon surface. A higher concentration of adsorbed species on the carbon surface facilitated the gasification of surface carbon oxides into carbon dioxide, and thus, an apparent mass drop associated with carbon loss was observed.

A similar corrosion behavior was observed when the XC-72 C-QCE was exposed to a continuous potential cycling between 0.1 V and 1.2 V at a scan rate of 50 mV s^{-1}, as shown in Fig. 5. The EQCM measurement revealed that carbon loss commenced at a higher potential in the early potential cycling state. Consistent with the decreased maximum mass gain that could be achieved during the successive CV scan, the potential corresponding to the onset of mass drop decreased and eventually stabilized at 1.04 V due to saturation of adsorbed species on the carbon surface. The corrosion rate decreased with time, as has been previously reported in several studies [10,25,26].

The carbon corrosion behavior under three fixed potentials, 0.4 V, 0.8 V and 1.2 V, respectively, is also investigated. Fig. 6 presents the EQCM mass change as a function of time for the XC-72 carbon support. The result exhibits minimum mass increment at 0.4 V and 0.8 V, and this is due to the fact that slow adsorption

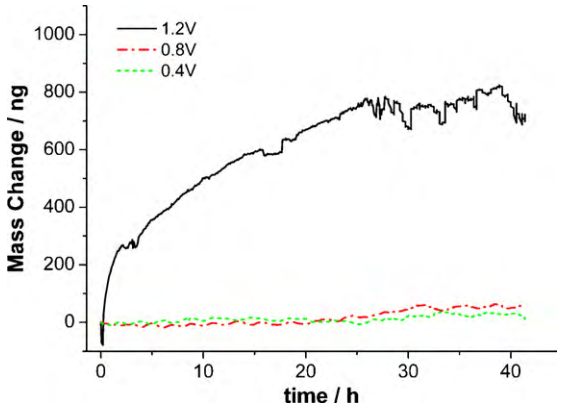

Fig. 6. EQCM mass change vs. time for the XC 72 carbon support as a function of specific potentials in deaerated 0.5 M H_2SO_4 at a temperature of 298 K.

of water, anions and surface oxides at such potentials. At 1.2 V, a decrease of mass is observed initially and such loss can be attributed to the CO_2 evolution. Afterward, a faster mass gain is seen due to the accumulation of oxides on the surface being faster than the formation of CO_2. The CO_2 formation rate rises initially and then decreases as a function of time as also reported by Oh et al. [12]. After 25 h of experiment at 1.2 V, the rate of increase slows down and a certain degree of oscillation was observed, and this may be due to saturation reached between mass consumption and generation on the carbon surface leading to a plateau.

It is worth to noting that the result between constant potential and cyclic voltammetry has distinct characteristic. The difference may be attributed to the difference in the carbon corrosion rate between potentiostatic and potentiodyanmic conditions. Shao et al. indicated that cycling of the oxidation/reduction of oxygen-containing species can enhance the carbon corrosion rate [27]. Maass et al. reported that the carbon corrosion rate at constant potential is much slower than in the potentiodyanmic mode due to insufficient activation energy [15], because the carbon corrosion is faster during potential cycling than the potentiostatic condition. In addition, potential cycling is also more closely related to the drive cycle operation of PEMFC on vehicle application. In this work we have employed the cyclic voltammetry method combing with EQCM to investigate carbon support corrosion.

3.2. Investigation of commercial carbon blacks

The commercial carbon blacks such as Vulcan XC-72, Ketjenblack ECP 300 and ECP 600, have been widely studied as carbon supports for PEMFCs. Although these carbon blacks have a similar structure and similar characteristics, there are some differences between them such as specific surface area, porosity and electrical conductivity. The carbon corrosion behaviors of these commercial fuel cell carbon supports were investigated in this study using EQCM measurements. Fig. 7 shows the corresponding mass change during the EQCM CV scan. A higher mass gain is observed on the ECP600 and ECP300 carbon electrodes, demonstrating higher BET

Table 1
BET data and EQCM results for XC-72, ECP300 and ECP600.

Carbon support	*Sn*[a] ($m^2\ g_c^{-1}$)	*S* ($m^2\ g_c^{-1}$)	Maximum mass gain (ng)	Max mass gain per area (ng cm^{-2})	Mass drop onset (V)	Mass drop rate[b] (ng $cm^{-2}\ s^{-1}$)
Vulcan XC-72	254	240	23.8	0.993	1.05	0.0115
Ketjenblack ECP300	950	890	81.9	0.920	1	0.0144
Ketjenblack ECP600	1270	1407	149.0	1.059	0.9	0.0245

[a] *Sn* is nominal BET value from manufactory.
[b] The mass drop rate was calculated by mass decrease within 0.1 V after mass drop onset.

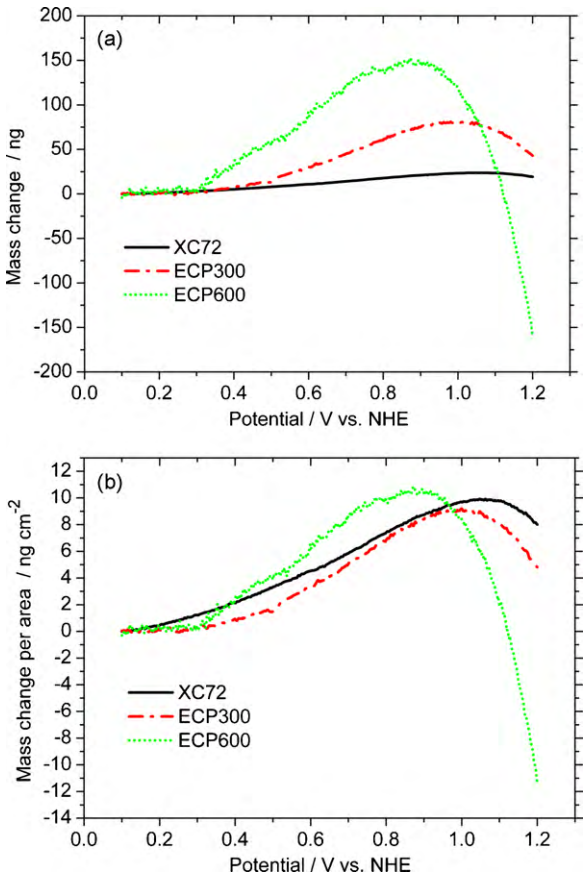

Fig. 7. EQCM mass change (positive CV scan) of (a) the original, and (b) normalized by the BET surface area for XC-72, ECP300 and ECP600 in deaerated 0.5 M H_2SO_4 at a scan rate of 10 mV s^{-1} and a temperature of 298 K.

surface area that could support more adsorbed species. As shown in Table 1, the maximum mass gains of the respective carbon support materials were as follows: ECP600 > ECP300 > XC-72, consistent with the BET values. The result listed in Table 1 is calculated from Fig. 7a, as the maximum mass per area is the maximum mass gain divided into the BET surface area. The mass drop rate is calculated as a decrease of mass within 0.1 V after the onset of the mass dropping. For example, the maximum mass gain of ECP600 is 149 ng, which is observed from the change of mass for the EQCM data from Fig. 7a. The BET surface area of ECP600 is 1407 $m^2\ g_c^{-1}$ and the weight of carbon is 10 μg. Given this, the maximum mass gain per area (ng cm^{-2}) can be calculated, and the mass drop rate of ECP600 can be calculated as (1.059–0.82 ng cm^{-2})/10 s.

The mass gain reversed and decreased in the high potential range, which is associated with carbon loss due to gasification of carbon surface oxides into carbon dioxide. The mass drop rate was also observed to follow the order of ECP600 > ECP300 > XC-72. This result revealed that higher amounts of adsorbed species in the carbon might enhance carbon corrosion during electrochemical oxidation. This result is consistent with that reported by Ball et al. [5], who reported that an increased wt% of carbon corroded with increasing BET surface area.

The carbon black materials exhibited a near maximum mass change when normalized by the respective BET surface area, implying a similar adsorption concentration on the specific surface area. However, the mass drop onset at 1.05 V, 1.0 V and 0.9 V was observed in the Vulcan XC-72, ECP300 and ECP600 samples, respectively. This potential corresponded to the onset of the mass drop decrease, suggesting a lower overvoltage for the gasification of surface carbon oxides. These results revealed that the high surface

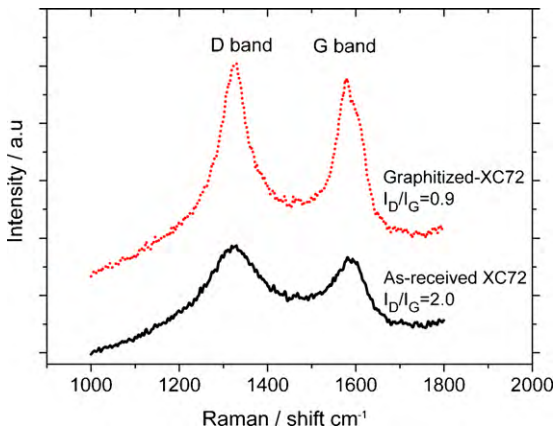

Fig. 8. Raman spectra of XC-72 and graphitized XC-72.

area of ECP300 and ECP600 carbon showed lower carbon corrosion-resistance than XC-72.

3.3. Influence of graphitization

Further improvement of carbon stability is needed to meet MEA performance and durability targets. Several studies have reported that using graphitized carbon supports is a material approach that achieves better corrosion stability [15,25,28]. In this study, we demonstrated the influence of graphitization on carbon support corrosion using the EQCM method.

Fig. 8 shows the Raman spectrum of the as-received XC-72 and the graphitized XC-72. The graphitization degree of carbon materials can be quantified from the Raman spectrum. The peak intensity I_D at ~1350 cm^{-1} (D-band) is an attribute of the defect structure of graphitic carbon. The peak intensity I_G at ~1580 cm^{-1} (G-band) is ascribed to the normal graphite structure [29]. Therefore, a lower value of I_D/I_G indicates better graphitization of the carbon materials. The graphitization and BET values of the XC-72 samples are presented in Table 2. The results showed that the as-received XC-72 acquired a notable increase in graphitization and strong decrease of the BET surface areas after graphitization treatment. The surface chemistry of the XC-72 before and after heat treatment was analyzed by using the XPS as shown in Fig. 9. The result shows that the O/C atomic ratio of XC-72 was decreased after heat treat. Accordingly, it is expected that the surface of graphitized carbon has became more hydrophobic.

As evident in Fig. 10, showing the EQCM result during the CV scan, the corresponding mass change was extremely low in the graphitized XC-72 carbon electrode. This result was attributed to the low BET surface area of the graphitized carbon. When taking into account the mass change normalized by the BET surface area, it was observed that the mass gain rate of graphitized XC-72 was still lower than that of the as-received XC-72. The mass gain of graphitized XC-72 occurred slowly, which was attributed to the hydrophobic surface and higher corrosion-resistance of the graphitized carbon. Hence, the mass drop onset potential of graphitized XC-72 occurred at a much higher potential (1.65 V) compared to the as-received XC-72 (1.05 V). The above results verify that the highly graphitized XC-72 shows excellent resistance to corrosion. The corrosion-resistance of the commercial

Table 2
The I_D/I_G and BET data for XC-72 and graphitized XC-72.

Carbon support	I_D/I_G	S ($m^2 g_c^{-1}$)
As-received XC-72	2.0	240
Graphitized XC-72	0.9	80

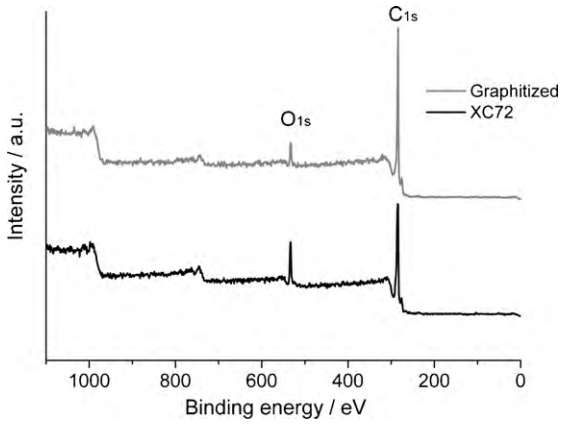

Fig. 9. XPS spectra of XC-72 before and after heat treatment.

carbon black support can be highly increased after graphitization treatment.

Multi-wall carbon nanotubes (MWNTs), with a unique cylinder graphitic structure, exhibit better properties than do most widely used commercial carbon supports, such as high electronic conductivity, a high specific surface area, excellent electronic conductivity and better electrochemical stability. These unique characteristics make MWNTs a potential alternative choice as a carbon support material in fuel cells. The carbon corrosion behavior of MWNTs was also investigated by EQCM in the present study. The I_D/I_G value of MWNTs is ~1.2, which is lower than that of as-received carbon black XC-72 (I_D/I_G = 2.0), indicating that MWNTs have a higher

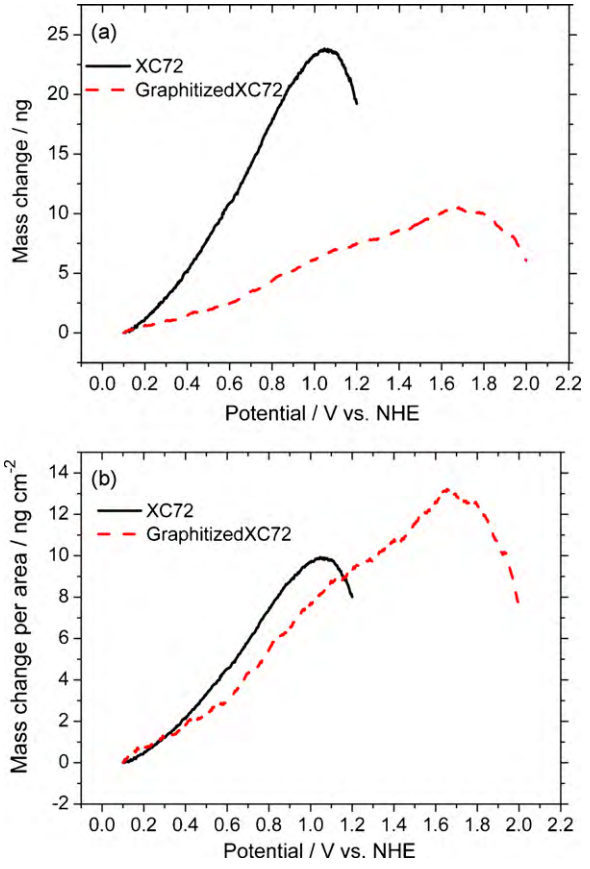

Fig. 10. EQCM mass change (positive CV scan) of (a) the original, and (b) normalized by the BET surface area for XC-72 and graphitized XC-72 in deaerated 0.5 M H_2SO_4 at a scan rate of 10 mV s^{-1} and a temperature of 298 K.

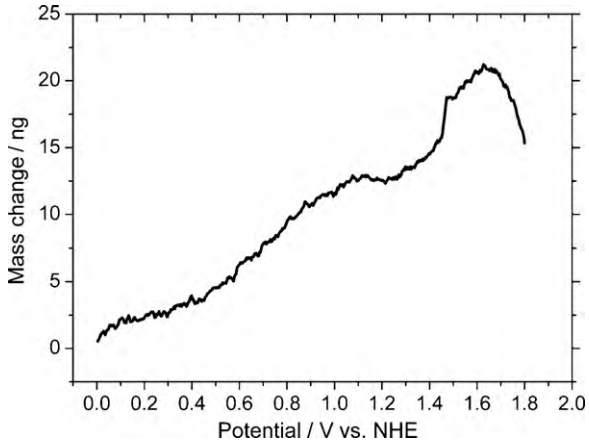

Fig. 11. EQCM mass change (positive CV scan) for MWNTs in deaerated 0.5 M H_2SO_4 at a scan rate of 10 mV s^{-1} and a temperature of 298 K.

degree of graphitization as compared to XC-72. The EQCM measurement results shown in Fig. 11 demonstrate that the mass drop onset potential of the MWNTs is ~1.62 V, which is similar to that of graphitized XC-72. This result further evidences that a highly ordered graphitic structure carbon such as graphitized XC-72 and MWNTs, possesses high corrosion-resistance in electrochemical environments.

4. Conclusions

1. Our study suggests that EQCM can be a simple and time-effective screening tool for evaluating the corrosion behavior of carbon supports in PEMFCs.
2. Carbon corrosion onset potential is observed at 1.04 V on Vulcan XC-72, 1.65 V on graphitized XC-72, 1.0 V on ECP300, 0.9 V on ECP600 and 1.62 V on MWNTs.
3. High amounts of surface carbon black show lower corrosion-resistance due to higher concentrations of adsorbed species on the carbon surface, which facilitates the gasification of surface carbon oxides into carbon dioxide.
4. The corrosion-resistance of XC-72 is improved after graphitization treatment.
5. MWNTs with highly ordered graphitic structures possess high corrosion-resistance.

Acknowledgements

This work was supported by the ITRI under project number 8254W0F100 and by the National Science Council of the Republic of China under contract number NSC98-2221-E-034-007-MY2.

References

[1] M. Sevilla, A.B. Fuertes, Carbon 44 (2006) 468–474.
[2] K. Kinoshita, J. Bett, Carbon 11 (1973) 237–247.
[3] H. Tang, Z. Qi, M. Ramani, J.F. Elter, J. Power Sources 158 (2006) 1306–1312.
[4] P.J. Ferreira, G.J. la O', Y. Shao-Horn, R. Makharia, H. Gasteiger, J. Electrochem. Soc. 152 (2005) A2256–A2271.
[5] S.C. Ball, S.L. Hudson, D. Thompsett, B. Theobald, J. Power Sources 171 (2007) 18–25.
[6] Y. Shao, G. Yin, Y. Gao, P. Shi, J. Electrochem. Soc. 153 (2006) 1093–1097.
[7] K. Kinoshita, Carbon: Electrochemical and Physicochemical Properties, Wiley, New York, 1988, 319.
[8] C.A. Reiser, L. Bregoli, T.W. Patterson, J.S. Yi, J.D. Yang, M.L. Perry, T.D. Jarvi, Electrochem. Solid-State Lett. 8 (2005) A273–A276.
[9] J.P. Meyers, R.M. Darling, J. Electrochem. Soc. 153 (2006) A1432–A1442.
[10] L. Li, Y. Xing, J. Electrochem. Soc. 153 (2006) A1823–A1828.
[11] L. Li, Y. Xing, J. Power Sources 178 (2008) 75–79.
[12] H.S. Oh, J.G. Oh, S. Haam, K. Arunabha, B. Roh, I. Hwang, H. Kim, Electrochem. Commun. 10 (2008) 1048–1051.

[13] L.M. Roen, C.H. Paik, T.D. Jarvi, Electrochem. Solid-State Lett. 7 (2004) A19–A22.
[14] A.M. Chaparro, N. Mueller, C. Atienza, L. Daza, J. Electroanal. Chem. 591 (2006) 69–73.
[15] S. Maass, F. Finsterwalder, G. Frank, R. Hartmann, C. Merten, J. Power Sources 176 (2008) 444–451.
[16] D.A. Buttry, in: A.J. Bard (Ed.), Electroanalytical Chemistry, vol. 17, Marcel Dekker, NY, 1991.
[17] A.P. Yadav, Y. Sugawara, A. Nishikata, T. Tsuru, ECS Trans. 16 (2008) 2093–2099.
[18] V.A.T. Dam, K. Jayasayee, F.A. deBruijn, Fuel Cells 9 (2009) 453–462.
[19] D.A. Buttry, M.D. Ward, Chem. Rev. 92 (1992) 1355–1379.
[20] K.H. Kangasniemi, D.A. Condit, T.D. Jarvi, J. Electrochem. Soc. 151 (2004) E125–E132.
[21] Y.Y. Shao, G.P. Yin, J. Zhang, Y.Z. Gao, Electrochim. Acta 51 (26) (2006) 5853–5857.
[22] M.J. Bleda-Martinez, D. Lozano-Castello, E. Morallon, D. Cazorla-Amoros, A. Linares-Solano, Carbon 44 (2006) 2642–2651.
[23] K. Kinoshita, J.A.S. Bett, Carbon 12 (1974) 525–533.
[24] N. Giordano, P.L. Antonucci, E. Passalacqua, L. Pino, A.S. Arico, K. Kinoshita, Electrochim. Acta 36 (1991) 1931–1935.
[25] P.T. Yu, W. Gu, R. Makharia, F.T. Wagner, H.A. Gasteiger, ECS Trans. 3 (2006) 797–809.
[26] M.F. Mathias, R. Makharia, H.A. Gasteiger, J.J. Conley, T.J. Fuller, C.J. Gittleman, S.S. Kocha, D.P. Miller, C.K. Mittelsteadt, T. Xie, S.G. Yan, P.T. Yu, Electrochem. Soc. Interface 14 (2005) 24–35.
[27] Y. Shao, J. Wang, R. Kou, M. Engelhard, J. Liu, Y. Wang, Y. Lin, Electrochim. Acta 54 (2009) 3109–3114.
[28] S. Ye, M. Hall, P. He, ECS Trans. 16 (2008) 2101–2113.
[29] D. Mattia, M.P. Rossi, B.M. Kim, G. Korneva, H.H. Bau, Y. Gogotsi, J. Phys. Chem. B. 110 (2006) 9850–9855.